Eur Radiol (2012) 22:2178–2185
DOI 10.1007/s00330-012-2477-3

HEPATOBILIARY-PANCREAS

Differentiation of neoplastic from bland macroscopic portal vein thrombi using dual-energy spectral CT imaging: a pilot study

Li Jun Qian · Jiong Zhu · Zhi Guo Zhuang · Qiang Xia · Yu Fan Cheng · Jian Ying Li · Jian Rong Xu

Received: 6 October 2011 / Revised: 14 March 2012 / Accepted: 22 March 2012 / Published online: 24 May 2012

Abstract
Objectives To assess the feasibility and value of dual-energy spectral computed tomography (DESCT) imaging for differentiating neoplastic from bland macroscopic portal vein (PV) thrombi.
Methods Computed tomography (CT) images of 44 patients with macroscopic PV thrombus (bland group, $n=16$; neoplastic group, $n=28$) were reviewed. Iodine-based material decomposition images in the portal venous phase were reconstructed to compare the iodine indices between groups, including thrombus iodine density (I_T), thrombus–aorta iodine density ratio (I_T/I_A), and thrombus–PV iodine density ratio (I_T/I_P). Differential diagnostic performances of DESCT were calculated in the subgroup of 21 patients with histopathological evidence (bland group, $n=12$; neoplastic group, $n=9$).
Results The iodine indices of the neoplastic group were significantly higher than those in the bland group ($P<0.001$). A threshold I_T of 1.14 mg/mL, I_T/I_A of 0.17, and I_T/I_P of 0.17 in the portal venous phase yielded 100 %, 88.9 %, and 100 % sensitivity, and 91.7 %, 91.7 %, and 83.3 % specificity, respectively, in differentiating neoplastic from bland PV thrombi.
Conclusions DESCT imaging with quantification of thrombus iodine density in the portal venous phase appears to be a promising new method for distinguishing neoplastic from bland macroscopic PV thrombi.
Key Points
- *Differentiating the nature of portal vein thrombus is of great clinical significance.*
- *Iodine-based material decomposition imaging reflects iodine distribution after contrast media administration.*
- *Dual-energy CT with iodine quantification can distinguish bland from neoplastic PV thrombi.*

Keywords X-ray computed tomography · Dual-energy CT · Thrombosis · Portal vein · Hepatocellular carcinoma

Abbreviations

CECT	contrast-enhanced CT
CDUS	colour Doppler ultrasound
DESCT	dual-energy spectral computed tomography
FN	false negative
FP	false positive
HCC	hepatocellular carcinoma
I_T	thrombus iodine density
I_T/I_A	thrombus–aorta iodine density ratio
I_T/I_P	thrombus–PV iodine density ratio
PV	portal vein
PVT	portal vein thrombosis
ROC	receiver operating characteristic
TP	true positive
TN	true negative

L. J. Qian · J. Zhu · Z. G. Zhuang · J. R. Xu (✉)
Department of Radiology, Renji Hospital,
Shanghai Jiaotong University School of Medicine,
No. 1630 Dongfang Rd. Pudong,
Shanghai 200127, People's Republic of China
e-mail: xujianr@gmail.com

Q. Xia
Department of Hepatic Surgery, Renji Hospital,
Shanghai Jiaotong University School of Medicine,
Shanghai 200127, People's Republic of China

Y. F. Cheng
Liver Transplantation Program, Chang Gung Memorial Hospital–Kaohsiung Medical Center,
Chang Gung University College of Medicine,
Kaohsiung 83305, Taiwan

J. Y. Li
CT Imaging Research Center, GE Healthcare China,
Beijing 100176, People's Republic of China

Introduction

Liver cirrhosis, hepatocellular carcinoma (HCC), and abdominal inflammation are the common causes of benign or malignant portal vein thrombosis (PVT) [1]. Neoplastic and bland thrombi can coexist, but they are formed through different pathophysiological mechanisms with differing prognoses. Bland thrombus, which develops from sluggish portal blood flow, is characterised by fibrin or blood clots without viable cells [2]. This type of thrombus can be resolved after thrombolytic and anticoagulant therapy. Conversely, neoplastic thrombi, which are often caused by the direct invasion of HCC into the portal vein (PV) [3, 4], are associated with early recurrence and intrahepatic metastasis after surgical resection [5, 6]. The presence of this type of thrombus is related to an advanced stage with a very limited probability of a cure. Thus, differentiating the nature of the thrombus is of great clinical significance in determining the therapeutic approach, predicting survival, and assessing candidates for liver transplantation.

Recently, dual-energy spectral CT (DESCT) imaging with material decomposition reconstruction has enabled the transformation of conventional attenuation data into effective material densities such as those of iodine and water. This procedure theoretically allows neoplastic thrombi to be differentiated on the basis of thrombus iodine density (I_T) after administering an iodine contrast agent because of the neovascularity of the thrombus. Thus, the present article aims to assess the feasibility and diagnostic value of DESCT imaging with iodine-based material decomposition in distinguishing neoplastic from bland thrombi.

Materials and methods

Subjects and study design

The study was approved by the ethics commission of our institution and written informed consent was obtained from each patient. The flow chart of the study design is shown in Fig. 1. From February 2010 to August 2011, 65 patients with confirmed or strongly suspected of having PVT by colour Doppler ultrasound (CDUS) were enrolled. The patients underwent multiphase contrast-enhanced CT (CECT) imaging with dual-energy spectral imaging in the portal venous phase to confirm the presence, nature and the underlying cause of the thrombi. The equilibrium phase was constantly checked to exclude streaming artefacts. Thirteen patients were excluded because of the following: (a) an absence of visible PV thrombi in the main PV trunk, and the first- and second-order branches under CECT; (b) a history of hepatic surgery, transarterial chemoembolisation, or percutaneous radiofrequency ablation; and (c) an unsuccessful examination resulted from body movement and artefacts.

The presence and the nature of PV thrombi were initially judged on the basis of conventional multiphase images without material decomposition reconstruction through the consensus of two experienced radiologists blinded to the clinical condition of the patients. The radiologists were asked to record in a tabular worksheet the presence or absence of each of the four characteristic CT features in Table 1 with a dichotomous score (1=presence, 0=absence) in each case [7, 8]. A five-grade CT features scale (from 0 to 4) was calculated by summation of the dichotomous scores in each case. This scale was considered to represent the overall confidence for thrombus characterisation using CECT imaging.

The criteria for neoplastic thrombi were (a) pathological proof, (b) presence of typical pulsatile arterial signals inside the thrombus under CDUS, (c) presence of at least two of the four characteristic CT features listed in Table 1. If the lesion met one of the three criteria, the final diagnosis of neoplastic PV thrombus was made. The criteria for bland thrombi were (a) pathologic proof, (b) none of the features listed in Table 1 were fulfilled and presence of evidence of shrinkage or stability of the thrombus during follow-up studies with at least 1-month interval. If the one of the two criteria was met, the thrombus was diagnosed as bland [9, 10]. Patients with coexisting bland and neoplastic thrombi were regarded as neoplastic cases, and only the thrombi with maximum cross-sectional diameters were evaluated in the case of multiple thrombi [11]. In 21 patients (9 neoplastic and 12 bland thrombi cases), who received en bloc hepatic resection or liver transplantation with an average gap period of 17.5 days, pathological results of the nature of PV thrombus were obtained. Eight patients were further excluded because the imaging findings were not sufficient enough to unequivocally differentiate neoplastic from bland thrombus. Thus, a total of 44 patients (34 men and 10 women) with a mean age of 52.5 years (range 33–88 years) formed the final study cohort. The 44 patients were diagnosed as having HCC (29 cases), hepatitis B- or C-related cirrhosis (12 cases), autoimmune cirrhosis (1 case), alcoholic cirrhosis (1 case), and colon cancer metastasis (1 cases).

DESCT imaging

Contrast-enhanced multiphase CT with dual energy in the portal venous phase was performed on a multi-detector CT (LightSpeed CT750 HD; GE Medical Systems, Milwaukee, WI, USA) in all patients. Arterial phase imaging was triggered using the bolus tracking technique (+100 HU above the baseline) after 100–120 mL of non-ionic iodinated contrast material (Iopamidol 370 mg/mL; Shanghai Bracco Sine Pharmaceutical Co., Ltd., Shanghai, China) was injected through the

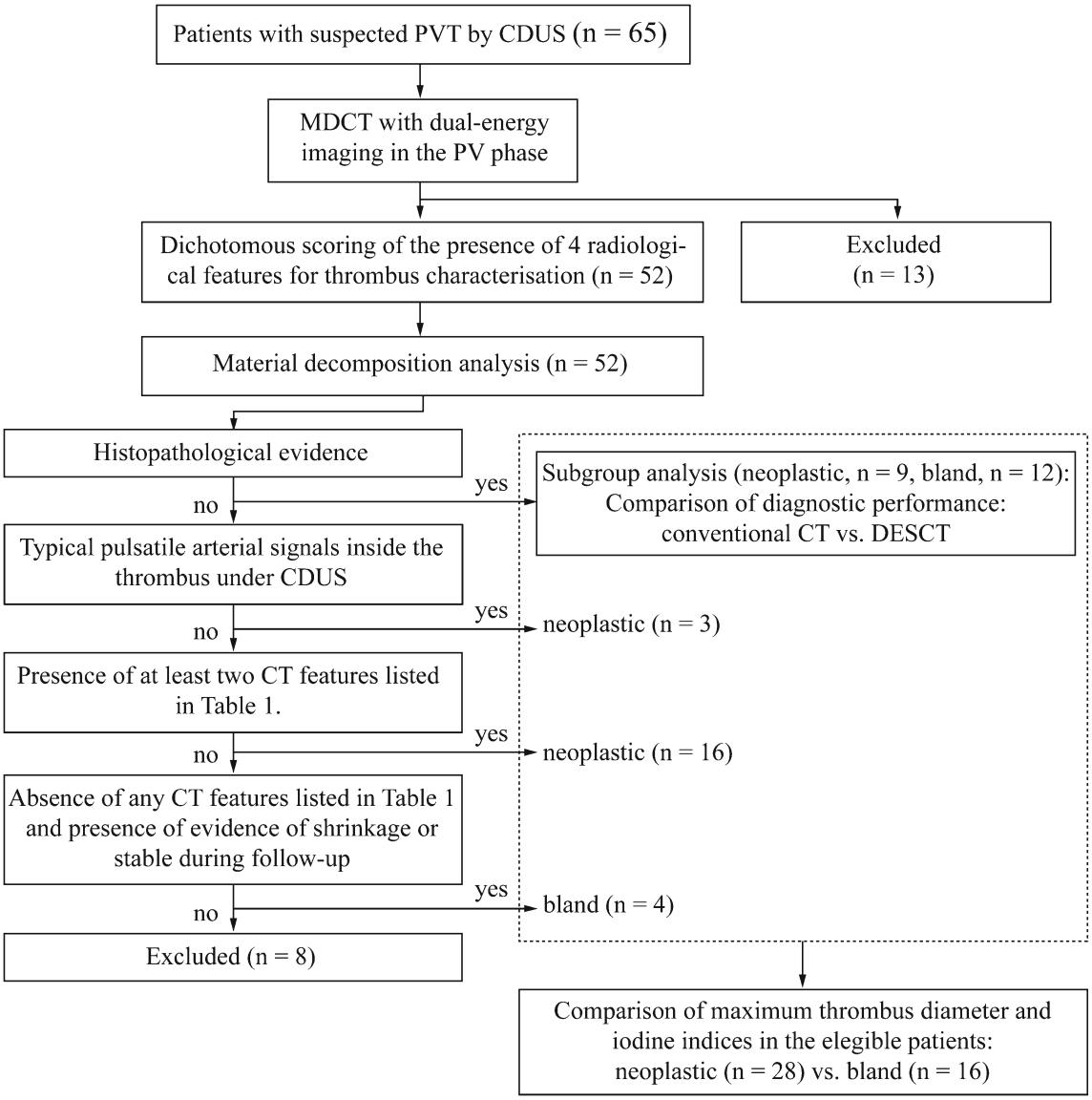

Fig. 1 Flow chart of the study design

Table 1 Characteristic CT features for differentiation of neoplastic from bland PVT

CT features
1. Direct infiltration of primary hepatic malignancy into the PV [7]
2. Expansion of the involved vessel or disproportionate enlargement compared with the unaffected same-order PV branches in the same lobe [8]
Main PV trunk: ≥2.6 cm
Right PV: ≥2.3 cm
Left PV: ≥2.2 cm
3. Arterial enhancement within the thrombus ≥20 HU [8]
4. Punctate or linear intrathrombus enhancement in the arterial phase CT images [7]

antecubital vein at a rate of 3–4 mL/s. This step was followed by portal venous and equilibrium phase imaging obtained with delays of 60 s and 140 s after the beginning of contrast medium injection. Dual-energy spectral imaging was performed in the portal venous phase using the following parameters: 0.8 s tube rotation time, 1.25 mm collimation, 600 mA tube current, 1.375 pitch, and 5 mm/5 mm slice thickness and interval for axial images, respectively. The estimated CT dose index derived from the imaging console for this portal venous phase DESCT acquisition was 18.28 mGy compared with 14.94 mGy for each conventional single-energy CECT.

Material decomposition and iodine density measurement

Material decomposition analysis was performed by consensus of the same two radiologists who performed the five-

grade scale scoring. Portal venous-phase polychromatic data acquired at 140 kVp and 80 kVp energy spectra, with 1.25 mm/1.25 mm slice thickness and interval, were reconstructed (Recon mode: Plus, GSI Recon image type: Mono) and transferred to a workstation (GE Advantage Workstation 4.4; GE Medical Systems) before the iodine and water material decomposition images were further generated using the iodine and water material pair with preset attenuation coefficients. The default monochromatic 70-keV axial images were reviewed to help localise the PV thrombi. Oval regions of interest (ROIs) ranging from 8.8 to 67.9 mm^2 were manually placed on axial monochromatic images within the centre of the thrombus, the adjacent PV trunk free of thrombi, and the aorta, respectively, while avoiding the vessel borders. The ROIs were automatically duplicated to the material decomposition images in exactly the same position and slice as they were placed in the monochromatic image. In the case of a heterogeneous PV thrombus, ROIs were placed predominantly in, but not limited to, the area with relatively high attenuation. To minimise inter-subject variations in iodine concentration derived from image timing and circulation status, the iodine density of the PV thrombi was normalised against that of the aorta (I_A) and the PV (I_P). The material decomposition results were compared between the groups in the entire study cohort (n=44). Diagnostic performances of conventional CT imaging and CT with dual-energy material decomposition in thrombus characterisation were compared between the groups in the subgroup of patients with histopathological evidence (n=21).

Statistical analysis

Statistical analysis was performed with MedCalc 11.6 (MedCalc Software, Mariakerke, Belgium). In the entire study cohort, the Mann–Whitney U test was used to compare the maximum cross-sectional diameters of thrombi between the bland and neoplastic groups, as well as I_Ts, the density ratio of the thrombus–aorta iodine (I_T/I_A) and thrombus–PV iodine (I_T/I_P) of the groups. In the subgroup of patients with histopathological evidence, the receiver operating characteristic (ROC) curves were drawn to establish the optimal threshold of CT features scale and iodine indices (i.e. I_T, I_T/I_A, and I_T/I_P) in distinguishing the nature of thrombi. Number of true positive (TP), true negative (TN), false positive (FP) and false negative (FN) cases, sensitivity, specificity, and the area under ROC curve (AUC) were calculated using the optimal thresholds. The overall differential diagnostic performances of CT features scale and iodine indices, in terms of AUC, were compared pairwise using DeLong analysis [12]. A P value less than or equal to 0.05 was regarded as statistically significant.

Results

There were 28 cases of neoplastic and 16 cases of bland PV thrombi in the entire study cohort, of which 9 neoplastic and 12 bland thrombi cases were histopathologically proven, respectively. The maximum thrombus diameter and the iodine indices (I_T, I_T/I_A, and I_T/I_P) of the neoplastic (n=28) and bland (n=16) groups in the entire study cohort are summarised in Table 2. The thrombus diameter and iodine indices observed from the neoplastic group were significantly higher than those of the bland group (Figs. 2, 3, and 4). In the subgroup of patients with histopathologically proven thrombi, the number of TP, TN, FP and FN cases, sensitivities, specificities, and AUCs at optimal thresholds of CT features scale and iodine indices are summarised in Table 3. When at least one CT feature in Table 1 was applied as the threshold, the sensitivity and specificity of the CECT characterisation of neoplastic from bland PVT were 88.9 % and 83.3 %, respectively. When at least two CT features were applied, the sensitivity and specificity were 66.7 % and 100 %, respectively. DESCT with material decomposition correctly characterised all but one case of bland thrombus with cavernous transformation of PV using $I_T > 1.14$ mg/mL as the optimal threshold. The overall differential diagnostic performances of iodine indices were slightly, but not significantly, greater than that of the CT features scale derived from conventional CECT imaging in the histopathologically proven population.

Table 2 Comparison of maximum thrombus diameter and iodine indices (I_T, I_T/I_A, and I_T/I_P) in the bland and neoplastic groups

	Maximum diameter of the thrombus (mm)	I_T	I_T/I_A	I_T/I_P
Neoplastic group (n=28)	16.12±6.37	2.67±0.98 mg/mL	0.35±0.11	0.37±0.15
Bland group (n=16)	12.51±5.00	0.92±0.31 mg/mL	0.12±0.05	0.12±0.05
Mann–Whitney U	137.00	6.00	10.00	12.00
*P	<0.05	<0.001	<0.001	<0.001

Data are means ± standard deviations

* $P \leq 0.05$ was regarded as statistically significant

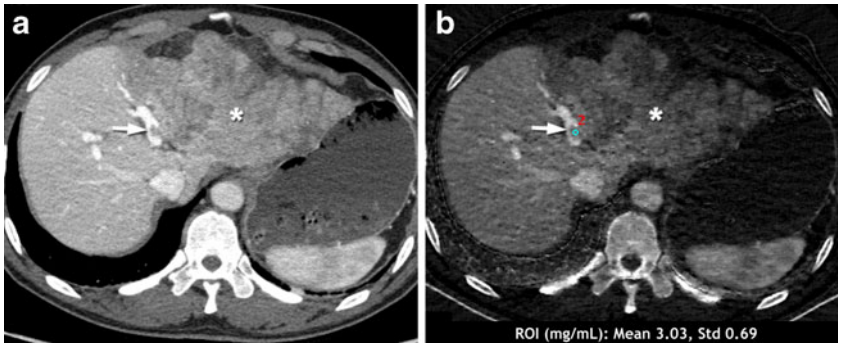

Fig. 2 Transverse monochromatic CT image (**a**) at 70 keV and iodine-based material decomposition image (**b**) depicting the direct infiltration of HCC (*) into the left branch of the PV with histopathologically proven neoplastic thrombus (*arrow*) formation in a 49-year-old man

Discussion

In recent studies, contrast-enhanced ultrasound appeared superior to both colour-Doppler ultrasound and spiral CT for the detection and characterisation of PVT [10, 13]. The main advantages of contrast-enhanced ultrasound (CEUS) over other modalities are that it is performed in real time and it has the ability to detect a small thrombus even in peripheral portal branches. However, the technique is observer-dependent and sometimes hampered by the presence of bowel gas [14]. Magnetic resonance imaging is of great value in the assessment of PVT [15, 16]. Recent reports have highlighted the potential of diffusion-weighted imaging to differentiate benign from malignant PV thrombus. However, MR is somewhat restricted by spatial resolution as well as lack of availability in some centres. A typical MR protocol with a slice thickness and interval of 5 mm/5 mm could potentially mask a small thrombus and might also be a source of error due to partial volume effects.

CECT imaging remains the principal investigation for the characterisation of PVT and its underlying cause. The imaging criteria for differentiating between malignant and benign thrombi using CT are well established. Tublin et al. [7] suggested that the presence of main PV dilation (≥23 mm) and intrathrombus enhancement is highly indicative of neoplastic PVT. Catalano et al. [8] showed that characteristic features such as intrathrombus arterial enhancement and PV expansion can be regarded as reference standards for differentiating between malignant and benign thrombi. However, PV thrombi are often barely visible on baseline unenhanced CT images, which might pose potential measuring problems in enhancement evaluation. Moreover, some thrombi manifest only subtle internal enhancement in the arterial phase. In the study by Tublin et al., dense punctate or linear intrathrombus enhancement was seen in only 43 % of patients with malignant PVT. In addition, the involvement of the extrahepatic portion of the PV by a tumour or thrombus may secondarily decrease the size of the intrahepatic component of the vein because of decreased blood flow [17]. Thus, intrathrombus arterial enhancement and expansion of the involved portal vessel might not always be observed in neoplastic PVT.

The use of dual-energy CT has been proposed to diagnose and quantify liver diseases such as fatty liver change or iron overload [18, 19]. The recent DESCT imaging allows materials within the object to be spectrally differentiated and quantified. For contrast-enhanced images, material decomposition isolates the iodinated contrast signal from the soft tissue to produce an iodine-based image series that provides information regarding the contrast material distribution in the organ [18, 20]. Kaza et al. [21] found that DESCT with iodine density measurement is highly specific in distinguishing enhancing from non-enhancing renal lesions. Neoplastic thrombi are characterised by abundant neovascularity with viable tumour cells, whereas bland thrombi are mainly composed of avascular fibrin or blood clots caused by the paucity of feeding vessels. Consequently, the iodine density of PV thrombi is theoretically associated with the degree of

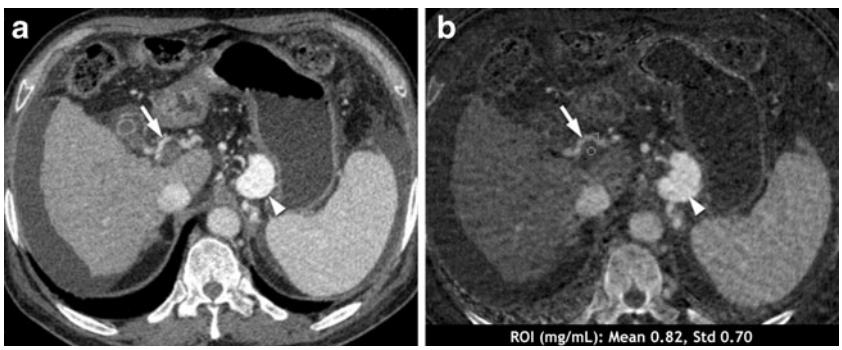

Fig. 3 Transverse monochromatic CT image (**a**) at 70 keV and iodine-based material decomposition image (**b**) depicting a bland PV thrombus (*arrow*) with low iodine density in a 58-year-old man with hepatitis B-related liver cirrhosis. A large retrogastric varix is also noted (*arrowhead*)

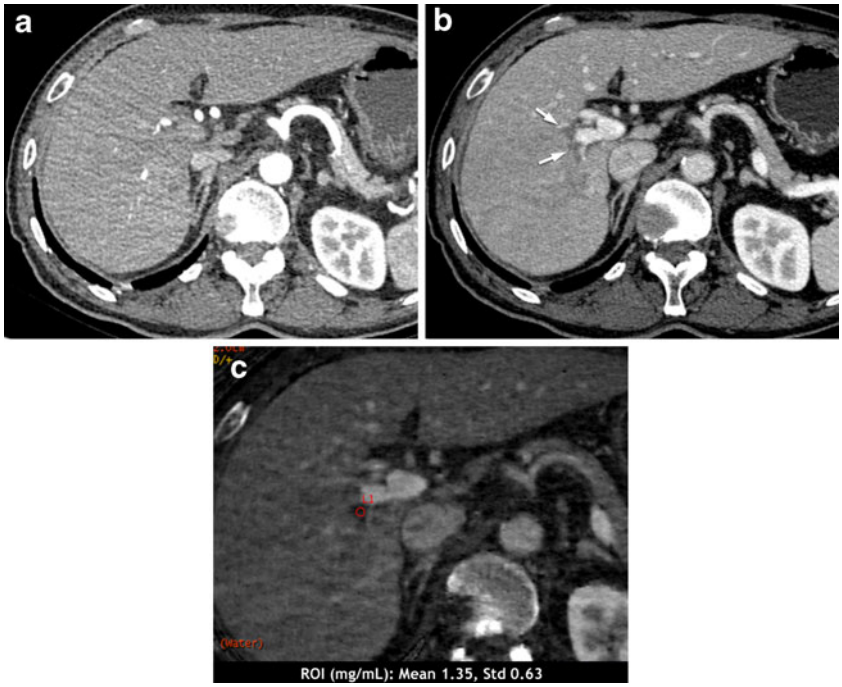

Fig. 4 Histopathologically proven neoplastic thrombi in a 64-year-old man with liver cirrhosis and superimposed HCC in segments V and VI (not shown). Transverse (**a**) arterial phase and (**b**) portal venous phase monochromatic CT images at 70 keV depicting the right anterior and posterior branches of PV thrombi (*arrows*) without clear evidence of HCC infiltration, arterial hypervascularity, or an expansile PV branch. (**c**) A relatively high intrathrombus iodine density is observed in the iodine-based material decomposition image

intrathrombus vascularity and can be further applied to distinguish the nature of the thrombi. This behaviour can explain the significant difference in the measured iodine density of neoplastic and bland thrombi in the results.

In the present study, the portal venous phase was chosen to study the I_T not only because of the ease in identifying thrombi in the portal venous phase, but also because the relationships between thrombi and primary hepatic lesions (if any) in the portal venous phase are more conspicuous than those in other phases. Compared with conventional CT imaging, PV thrombus differentiation using iodine-based material decomposition allows the straightforward evaluation of intrathrombus enhancement regardless of the diameter of the affected vessels and the extent of arterial enhancement. Noticeably, in tissues that do not contain the selected materials (e.g. iodine and water density measured in the skeletal bone), the material density mathematically represents the amount of each material necessary to produce the equivalent attenuation coefficient observed at low and high kV spectra, rather than the exact concentration of the selected materials.

Iodine density in the neoplastic thrombus might vary with the contrast uptake and enhancement degree of the thrombus. Poor intrathrombus enhancement in the PV phase derived from intratumour necrosis, fibrosis, or fatty metamorphosis can lead to false negatives [22]. Similarly, enhancing portal channels do not always signify neoplastic thrombus. Although we did not encounter it in our study, non-neoplastic PV thrombosis can occur where partial venous recanalisation in the presence of severe portal hypertension and reversed flow can lead to enhancing channels within the

Table 3 Differential diagnostic performance of CT features scale, I_T, I_T/I_A, and I_T/I_P in distinguishing neoplastic from bland PV thrombi in the subgroup of patients with histopathologically proven thrombi (n=21)

	Optimal threshold	TP	TN	FP	FN	Sensitivity (%)	Specificity (%)	AUC
CT features scale	Presence of at least one CT feature	8	10	2	1	88.9	83.3	0.91
I_T	>1.14 mg/mL	9	11	1	0	100	91.7	0.95
I_T/I_A	>0.17	8	11	1	1	88.9	91.7	0.92
I_T/I_P	>0.17	9	10	2	0	100	83.3	0.93
Significance level by pairwise comparison of the ROC curve*	I_T vs. I_T/I_A, P=0.82		I_T vs. CT features scale, P=0.64					
	I_T vs. I_T/I_P, P=0.80		I_T/I_A vs. CT features scale, P=0.82					
	I_T/I_A vs. I_T/I_P, P=0.60		I_T/I_P vs. CT features scale, P=0.90					

AUC area under the curve, *ROC* receiver operating characteristic

* $P \leq 0.05$ was regarded as statistically significant

thrombosed vein in the early venous phase, which can in turn mimic tumour neovascularity. In addition, in the case of chronic PV occlusion with cavernous transformation, thrombus can be misinterpreted as enhancing due to the enhancing vessel walls or the partial volume effects with superimposed periportal collaterals, especially when the PV itself is hardly discriminable. Therefore, conventional CECT is still crucial in the detection and characterisation of PV thrombi. On the other hand, the detectability of PV thrombi largely depends on their size. CECT is generally accepted as a reliable tool in identifying and characterising macroscopic PV thrombus, whereas CT has lower sensitivity in detecting and characterising small peripheral neoplastic thrombi that are continuous with and isointense to the tumour mass when compared with CEUS [10]. In the current study, only the macroscopic thrombi visible on CECT were analysed; hence, the exact detection accuracy of DESCT remains unclear. Several articles indicated improved DESCT performance in identifying or characterising small hepatic lesions compared with conventional CT [23, 24]. Whether or not DESCT improves the detection and characterisation of minute thrombi remains to be evaluated.

The current study has several limitations. First, the nature of the thrombi was judged on the basis of clinical and imaging findings rather than histopathological evidence from 23 cases (52.3 %). Ultrasound-guided fine-needle biopsy is useful in establishing the benignity or malignancy of PVT [25]. However, this invasive procedure is usually contraindicated in the presence of impaired blood coagulation among patients with advanced cirrhosis. Moreover, in patients with hepatic malignancy, seeding of the tumour may occur along the needle track [2]. With the limited histopathologically proven cases, the overall differential diagnostic performance of DESCT with material decomposition and that of conventional CT imaging did not reach significant difference. Nevertheless, it is conceivable that iodine-based material decomposition may provide some information on the condition of neoplastic thrombi without vessel expansion and obvious arterial contrast enhancement, or bland thrombi with remarkable vessel expansion. Whether DESCT provides added value in PV thrombi characterisation is still undefined in this pilot study. Further study with a larger study population or different reference standard will be helpful in answering this question better. Second, observers could distinguish the thrombi from the images, which might affect the iodine density measurement. Third, only the thrombi visible on CT, with maximum diameters, were evaluated for multiple PV thrombi presentation. Considering that the ROI of small lesions might be vulnerable to measurement error, the accuracy of macroscopic PV thrombus characterisation using iodine density measurement in the portal venous phase might have been overestimated. Fourth, in the present study, the intersubject variation derived from these factors was avoided by normalising I_T against I_A and I_P. Given the complexity of hepatic haemodynamics, this simplified normalisation method is far from optimal because it cannot eliminate the mutual influences of the arterial and portal blood supply.

At present, there are three different approaches to clinical dual-energy CT commercially available: DESCT via rapid voltage switching, dual-source CT, and dual-layer ('sandwich') detector CT [26]. The differences in physical structure for dual-energy implementation and material decomposition algorithm between vendors might produce a slightly different but statistically significant variability in iodine density values [27–30]. Therefore, the cut-off value used for PV thrombus characterisation in the present study is dependent on the CT system and protocol rather than a universal value. In this study, an increased radiation exposure in the portal venous phase was recorded by applying dual-energy scan compared to that recorded using conventional CT imaging. This finding might be due to the unavailability of the adaptive modulation of tube current when rapid voltage switching was performed [27]. Replacing true unenhanced images with virtual unenhanced images or using focused dual-energy acquisition was reported to be useful to reduce radiation exposure [31, 32]. In addition, alternative low-dose approaches can be obtained in the future with photon counting detectors. These detectors can be used to detect and classify spectral 'k-edge' patterns of clinically relevant materials at very low concentrations, given that a high enough count rate can be achieved for clinical use [26].

In summary, contrast-enhanced DESCT imaging with quantification of thrombus iodine density in the portal venous phase appears to be a promising new method for distinguishing neoplastic from bland macroscopic PV thrombi. However, the added value of this novel technology in this entity still requires further validation.

Acknowledgments J.Y.L. is an employee if GE Healthcare, the manufacturer of the CT system used in this study. The work was partially funded by the Shanghai Leading Academic Discipline Project (S30203) and the Scientific Program of Shnaghai Jiaotong University School of Medicine (YZ1004).

References

1. Parvey HR, Raval B, Sandler CM (1994) Portal vein thrombosis: imaging findings. AJR Am J Roentgenol 162:77–81
2. Piscaglia F, Gianstefani A, Ravaioli M et al (2010) Criteria for diagnosing benign portal vein thrombosis in the assessment of patients with cirrhosis and hepatocellular carcinoma for liver transplantation. Liver Transpl 16:658–667
3. Marn CS, Francis IR (1992) CT of portal venous occlusion. AJR Am J Roentgenol 159:717–726
4. Lee HK, Park SJ, Yi BH, Yeon EK, Kim JH, Hong HS (2008) Portal vein thrombosis: CT features. Abdom Imaging 33:72–79

5. Shah SA, Greig PD, Gallinger S et al (2006) Factors associated with early recurrence after resection for hepatocellular carcinoma and outcomes. J Am Coll Surg 202:275–283
6. Portolani N, Coniglio A, Ghidoni S et al (2006) Early and late recurrence after liver resection for hepatocellular carcinoma: prognostic and therapeutic implications. Ann Surg 243:229–235
7. Tublin ME, Dodd GD 3rd, Baron RL (1997) Benign and malignant portal vein thrombosis: differentiation by CT characteristics. AJR Am J Roentgenol 168:719–723
8. Catalano OA, Choy G, Zhu A, Hahn PF, Sahani DV (2010) Differentiation of malignant thrombus from bland thrombus of the portal vein in patients with hepatocellular carcinoma: application of diffusion-weighted MR imaging. Radiology 254:154–162
9. Dodd GD 3rd, Memel DS, Baron RL, Eichner L, Santiguida LA (1995) Portal vein thrombosis in patients with cirrhosis: does sonographic detection of intrathrombus flow allow differentiation of benign and malignant thrombus? AJR Am J Roentgenol 165:573–577
10. Rossi S, Ghittoni G, Ravetta V et al (2008) Contrast-enhanced ultrasonography and spiral computed tomography in the detection and characterization of portal vein thrombosis complicating hepatocellular carcinoma. Eur Radiol 18:1749–1756
11. Tarantino L, Francica G, Sordelli I et al (2006) Diagnosis of benign and malignant portal vein thrombosis in cirrhotic patients with hepatocellular carcinoma: color Doppler US, contrast-enhanced US, and fine-needle biopsy. Abdom Imaging 31:537–544
12. DeLong ER, DeLong DM, Clarke-Pearson DL (1988) Comparing the areas under two or more correlated receiver operating characteristic curves: a nonparametric approach. Biometrics 44:837–845
13. Rossi S, Rosa L, Ravetta V et al (2006) Contrast-enhanced versus conventional and color Doppler sonography for the detection of thrombosis of the portal and hepatic venous systems. AJR Am J Roentgenol 186:763–773
14. Bradbury MS, Kavanagh PV, Bechtold RE et al (2002) Mesenteric venous thrombosis: diagnosis and noninvasive imaging. Radiographics 22:527–541
15. Kreft B, Strunk H, Flacke S et al (2000) Detection of thrombosis in the portal venous system: comparison of contrast-enhanced MR angiography with intraarterial digital subtraction angiography. Radiology 216:86–92
16. Akin O, Dixit D, Schwartz L (2011) Bland and tumor thrombi in abdominal malignancies: magnetic resonance imaging assessment in a large oncologic patient population. Abdom Imaging 36:62–68
17. Shah ZK, McKernan MG, Hahn PF, Sahani DV (2007) Enhancing and expansile portal vein thrombosis: value in the diagnosis of hepatocellular carcinoma in patients with multiple hepatic lesions. AJR Am J Roentgenol 188:1320–1323
18. Yeh BM, Shepherd JA, Wang ZJ, Teh HS, Hartman RP, Prevrhal S (2009) Dual-energy and low-kVp CT in the abdomen. AJR Am J Roentgenol 193:47–54
19. Goldberg HI, Cann CE, Moss AA, Ohto M, Brito A, Federle M (1982) Noninvasive quantitation of liver iron in dogs with hemochromatosis using dual-energy CT scanning. Invest Radiol 17:375–380
20. Fletcher JG, Takahashi N, Hartman R et al (2009) Dual-energy and dual-source CT: is there a role in the abdomen and pelvis? Radiol Clin North Am 47:41–57
21. Kaza RK, Caoili EM, Cohan RH, Platt JF (2011) Distinguishing enhancing from nonenhancing renal lesions with fast kilovoltage-switching dual-energy CT. AJR Am J Roentgenol 197:1375–1381
22. Tajima T, Honda H, Taguchi K et al (2002) Sequential hemodynamic change in hepatocellular carcinoma and dysplastic nodules: CT angiography and pathologic correlation. AJR Am J Roentgenol 178:885–897
23. Lv P, Lin XZ, Li J, Li W, Chen K (2011) Differentiation of small hepatic hemangioma from small hepatocellular carcinoma: recently introduced spectral CT method. Radiology 259:720–729
24. Altenbernd J, Heusner TA, Ringelstein A, Ladd SC, Forsting M, Antoch G (2011) Dual-energy-CT of hypervascular liver lesions in patients with HCC: investigation of image quality and sensitivity. Eur Radiol 21:738–743
25. Vilana R, Bru C, Bruix J, Castells A, Sole M, Rodes J (1993) Fine-needle aspiration biopsy of portal vein thrombus: value in detecting malignant thrombosis. AJR Am J Roentgenol 160:1285–1287
26. Johnson TRC, Kalender WA (2011) Physical background. In: Johnson TRC, Fink C, Schönberg SO, Reiser MF (eds) Dual energy CT in clinical practice. Springer, Berlin, pp 3–9
27. Silva AC, Morse BG, Hara AK, Paden RG, Hongo N, Pavlicek W (2011) Dual-energy (spectral) CT: applications in abdominal imaging. Radiographics 31:1031–1046
28. Johnson TR, Krauss B, Sedlmair M et al (2007) Material differentiation by dual energy CT: initial experience. Eur Radiol 17:1510–1517
29. Zussman BM, Boghosian G, Gorniak RJ et al (2011) The relative effect of vendor variability in CT perfusion results: a method comparison study. AJR Am J Roentgenol 197:468–473
30. Stadler A, Schima W, Prager G et al (2004) CT density measurements for characterization of adrenal tumors ex vivo: variability among three CT scanners. AJR Am J Roentgenol 182:671–675
31. Coursey CA, Nelson RC, Boll DT et al (2010) Dual-energy multidetector CT: how does it work, what can it tell us, and when can we use it in abdominopelvic imaging? Radiographics 30:1037–1055
32. Ascenti G, Siragusa C, Racchiusa S et al (2010) Stone-targeted dual-energy CT: a new diagnostic approach to urinary calculosis. AJR Am J Roentgenol 195:953–958